BNL-209653-2018-JAAM

Mechanistic Insights into Electrochemical Nitrogen Reduction Reaction on Vanadium Nitride Nanoparticles

X. Yang, J. G. Chen

To be published in "JOURNAL OF THE AMERICAN CHEMICAL SOCIETY"

October 2018

Chemistry Department

Brookhaven National Laboratory

U.S. Department of Energy

USDOE Office of Science (SC), Basic Energy Sciences (BES) (SC-22)

Notice: This manuscript has been authored by employees of Brookhaven Science Associates, LLC under Contract No. DE-SC0012704 with the U.S. Department of Energy. The publisher by accepting the manuscript for publication acknowledges that the United States Government retains a non-exclusive, paid-up, irrevocable, world-wide license to publish or reproduce the published form of this manuscript, or allow others to do so, for United States Government purposes.

DISCLAIMER

This report was prepared as an account of work sponsored by an agency of the United States Government. Neither the United States Government nor any agency thereof, nor any of their employees, nor any of their contractors, subcontractors, or their employees, makes any warranty, express or implied, or assumes any legal liability or responsibility for the accuracy, completeness, or any third party's use or the results of such use of any information, apparatus, product, or process disclosed, or represents that its use would not infringe privately owned rights. Reference herein to any specific commercial product, process, or service by trade name, trademark, manufacturer, or otherwise, does not necessarily constitute or imply its endorsement, recommendation, or favoring by the United States Government or any agency thereof or its contractors or subcontractors. The views and opinions of authors expressed herein do not necessarily state or reflect those of the United States Government or any agency thereof.

Mechanistic Insights into Electrochemical Nitrogen Reduction Reaction on Vanadium Nitride Nanoparticles

Xuan Yang,[†,‡] Jared Nash,[†,‡] Jacob Anibal,[†] Marco Dunwell,[†] Shyam Kattel,[§,#] Eli Stavitski,[¶] Klaus Attenkofer,[¶] Jingguang Chen,[§,#,*] Yushan Yan,[†,*] and Bingjun Xu[†,*]

[†]Center for Catalytic Science and Technology, Department of Chemical and Biomolecular Engineering, University of Delaware, 150 Academy Street, Newark DE, 19716

[¶]National Synchrotron Light Source II, Brookhaven National Laboratory, Upton, New York 11973, United States

[§]Chemistry Division, Brookhaven National Laboratory, Upton, NY 11973, USA

[#]Department of Chemical Engineering, Columbia University, New York, NY 10027, USA.

[‡]These authors contributed equally to this work.

[*]Address correspondence to jgchen@columbia.edu, yanys@udel.edu, and bxu@udel.edu

Contents

1. Experimental Methods

1.1. Chemicals and Materials

1.2. Synthesis of Vanadium Nitride Nanoparticles

1.3. Characterizations of Catalysts

1.4. Preparation of MEA and Procedure for ENRR Tests

2. Quantification of Ammonia

3. Nitrogen Reduction in Batch Mode under $^{15}N_2$

4. Deconvolution of XPS Spectra

5. *Operando* XAS Characterizations of the Catalysts

6. Production Rate and FE of Other ENRR Catalysts

7. Computational Methods

8. Procedure for Turnover Number Calculations

1. Experimental Methods

1.1. Chemicals and Materials

Pt/C [46 weight percent (wt%) Pt supported on Ketjen Black, Tanaka Kikinzoku Kogyo] was obtained commercially and used as received. Particle sizes and distributions of the commercial Pt/C were examined in our previous paper under a transmission electron microscope (TEM, JEOL 2010F, 200 kV).[1] Urea (98%), vanadium oxychloride (99%), Potassium hydroxide (KOH, 99.99%), sulfuric acid (H_2SO_4, 99.999%), D_2O (99.9%), and dimethyl sulphoxide (DMSO, 99.99%) were purchased from Sigma-Aldrich. Ammonium sulfate ($(NH_4)_2SO_4$, 99.5%) was obtained from Acros Organics. Ethanol (100%) was purchased from Decon Laboratories, Inc. Isopropanol (IPA, 99.9%) was obtained from Fisher Chemical. Nafion (LQ-1105-1100 EW, 5 wt%), Nafion-211 membrane, and carbon paper (Sigracet 39 BC) were all purchased from Fuel Cell Store. Nessler's reagents were obtained from HANNA Instruments. Tin boats for Elementar analysis were purchased from EA Consumables, Inc. $^{15}N_2$ (98 atom % ^{15}N) was purchased from Cambridge Isotope Laboratories, Inc.

1.2. Synthesis of Vanadium Nitride Nanoparticles

Vanadium nitride nanoparticles were synthesized following a "urea-glass" method.[2] Typically, 1 g of vanadium precursor was dissolved in 2 g of ethanol to make the dark-reddish precursor solution; then 1.04 g of urea was slowly added into the alcoholic solution; the dispersion was stirred until urea was completely solubilized and the solution changed from dark-reddish to green; the solution was then dried into a glass or glassy film by evaporating the solvent; the gel was then put into an furnace under a N_2 flow at 800 °C for 3 h with a heating ramp of 3 °C/min.

1.3. Characterizations of Catalysts

Brunauer-Emmett-Teller (BET) surface area measurements were collected on a Micromeritics ASAP 2020 analyzer. Scanning electron microscopy (SEM) images were taken using Zeiss Auriga 60 CrossBeam. Transmission electron microscopy (TEM) images were taken using a JEOL JEM 3010 TEM microscope (Germany). X-ray diffraction (XRD) patterns were collected using a Bruker D8 XRD operating instruction with a Cu K_α X-ray tube. X-ray photoelectron spectroscopy (XPS) measurements were completed on each sample with a Thermo Scientific K-Alpha spectrometer. Each spectrum was collected with

a spot size of 400 μm and an operating pressure of less than 3.0×10^{-7} Pa using an Al Kα microfused monochromatized source (1486.6 eV) with a resolution of 0.1 eV. X-ray photoelectron spectra were analyzed using the Avantage Data System, a software package available through Thermo Scientific. UV−vis absorption spectra were recorded with a Cary 60 spectrometer (Agilent Technologies). Thermogravimetric analysis (TGA) was performed in air atmosphere on a TA Discovery TGA instrument. The elementar analysis was performed on a CHNS Elementar vario EL cube. *Operando* electrochemical X-ray absorption spectroscopic (XAS) experiments were conducted at Beamline 8-ID, National Synchrotron Light Source II, Brookhaven National Laboratory.

The N and C contents in the fresh VN catalysts were determined to be 15.51 ± 0.01 wt% and 16.85 ± 0.01 wt%, respectively, using CHNS Elementar (Table S1-1). The CHNS Elementar analysis of each sample was repeated five times and the relatively small deviation demonstrated the good reproducibility. The XPS results revealed the existence of multiple nitride, oxynitride, and oxide species on the surface of VN nanoparticles (Figure S1-2). All the XPS spectra in this work were deconvoluted using the same set of parameters (Section 4). Thermogravimetric analysis (TGA) was employed to confirm the amount of V and C in the catalysts, respectively. There were two weight loss (negative) peaks at around 200 °C and 400 °C in the TGA curve (Figure S1-3), corresponding to the loss of water and carbon, respectively. When the temperature was above 200 °C, VN was oxidized into brown/yellow solid, indicating the formation of V_2O_5, which was confirmed by XRD (Figure S1-4). The composition of the fresh VN catalysts was determined to be 60.0 wt% of V, 20.0 wt% of N and 20.0 wt% of C, which were consistent with the CHNS Elementar analysis.

1.4. Preparation of MEA and Procedure for ENRR Tests

The chemical stability of VN nanoparticles is investigated by soaking as-synthesized VN nanoparticles in 1 M H_2SO_4 at 85 °C. UV-vis spectra were collected to monitor the concentration of VO^{2+} in the solution and thus the degradation rate of VN nanoparticles. Roughly 7% of V in the VN nanoparticles was leached out within the first hour (Figure S1-5), which was attributed to the dissolution of surface vanadium oxides. The degradation slowed down after 1 h and a total of ~12% of V was dissolved within 24 h. Prior to

reactivity studies, as-synthesized VN nanoparticles were soaked in 1 M H_2SO_4 at 85 °C for 1 h.

The ink solutions of VN catalysts were mixed into a mixture of H_2O:IPA (50:50) with 30 wt% Nafion ionomer and hand-sprayed onto carbon paper to an approximate metal loading of 0.5 mg cm^{-2} to serve as the cathode. The ink solution of Pt/C was prepared following the same procedure outlined above and was subsequently sprayed onto a Nafion-211 membrane using a Sonotek sprayer to reach a final Pt loading of 0.4 mg cm^{-2}, which was used as the anode. After hot-pressed at 140 °C for 3 min, the membrane electrode assembly (MEA) was fabricated for electrochemical nitrogen reduction reaction (ENRR). The anode was fed with 1 atm of H_2, which effectively functioned as a RHE. Thus, the cell potential is numerically identical to the cathode potential versus RHE and the ENRR can be performed at well-defined potentials. The membrane was then covered with a Sigracet 39 BC carbon paper anode gas diffusion layer and assembled with the cathode into an MEA with an active geometric cross-sectional area of 5 cm^2 (Figure S1-6). The production of ammonia was conducted with the cathode and anode fed by high-purity N_2 (99.999%) and H_2 (99.999%) under 1 atm at a constant flow rate of 0.1 L min^{-1}, respectively. The temperature of the cell was maintained at 80 °C. The temperatures of the humidifiers for cathode and anode were controlled to be 85 °C to maintain 100% relative humidity in the electrolyzer. The ammonia produced on the cathode and anode were collected in 1 mM H_2SO_4. After the tests in a PEMEL, the MEA was soaked in 3 M H_2SO_4 for 24 h to extract the ammonia inside the membrane.

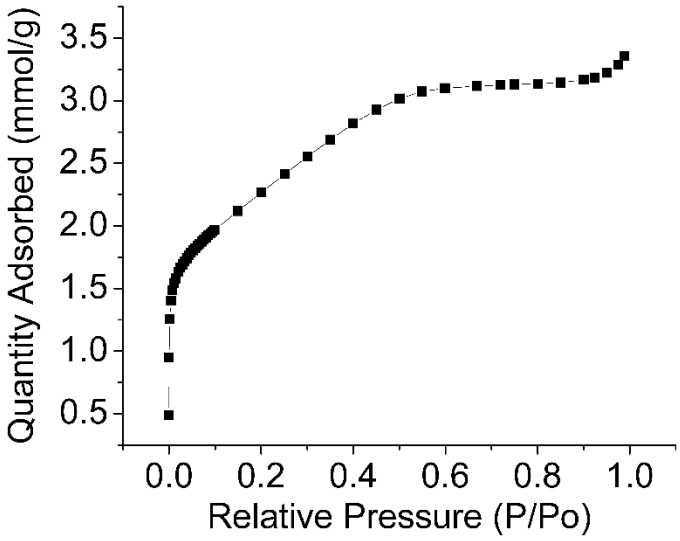

Figure S1-1. Nitrogen adsorption isotherm for VN nanoparticles. The Brunauer−Emmett−Teller (BET) surface area is 177 m^2 g^{-1}.

Table S1-1. The CHNS Elementar analysis results of VN nanoparticles.

Sample	N content (wt%)	C content (wt%)
VN nanoparticles	15.51 ± 0.01	16.85 ± 0.01

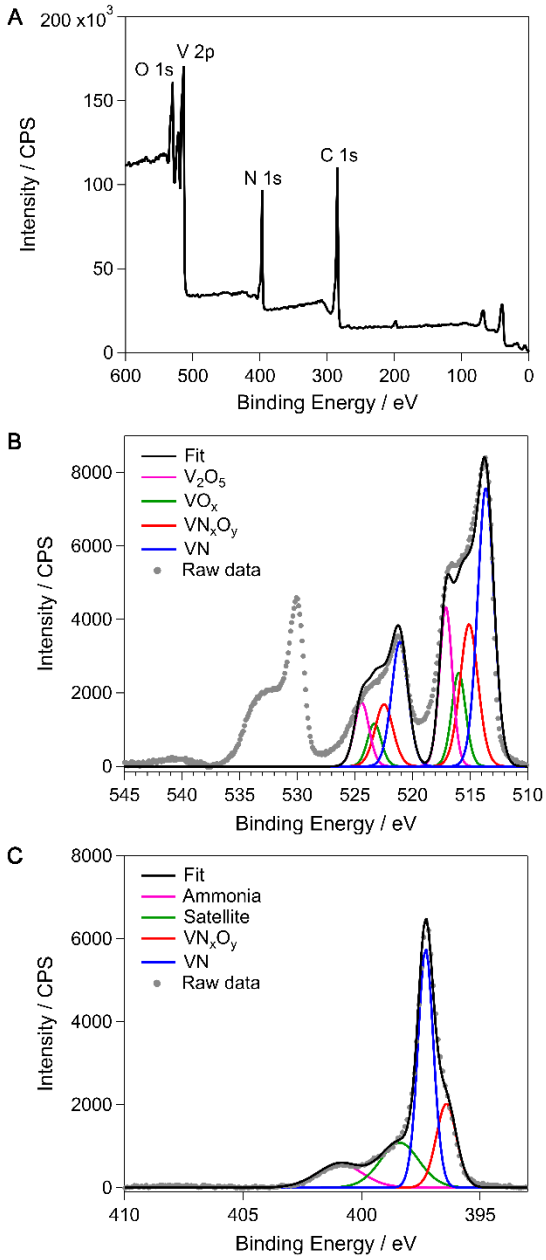

Figure S1-2. (A) XPS survey spectrum of VN nanoparticles. (B) XPS deconvolutions of the V 2p region. The five peaks in the V 2p region are attributed to VN, VN_xO_y, VO_x, and V_2O_5 from lower to higher binding energy, respectively. (C) XPS deconvolutions of the N 1s region. The four peaks in the N 1s region are attributed to VN_xO_y, VN, satellite feature, and ammonia from lower to higher binding energy, respectively.

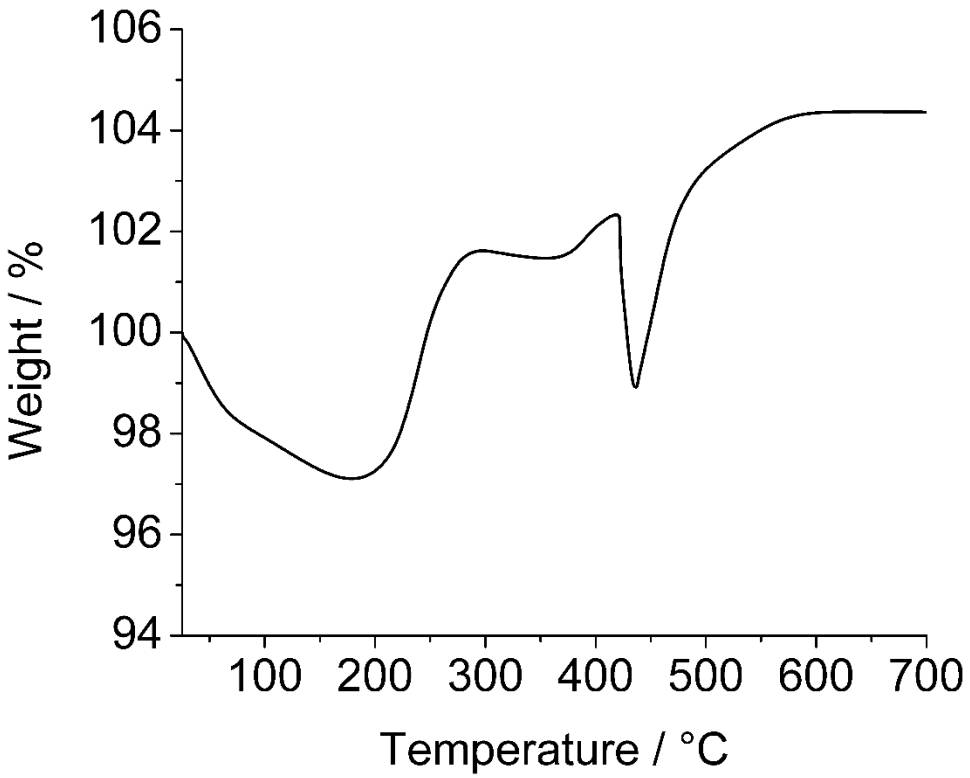

Figure S1-3. Thermogravimetric analysis (TGA) curve of VN nanoparticles.

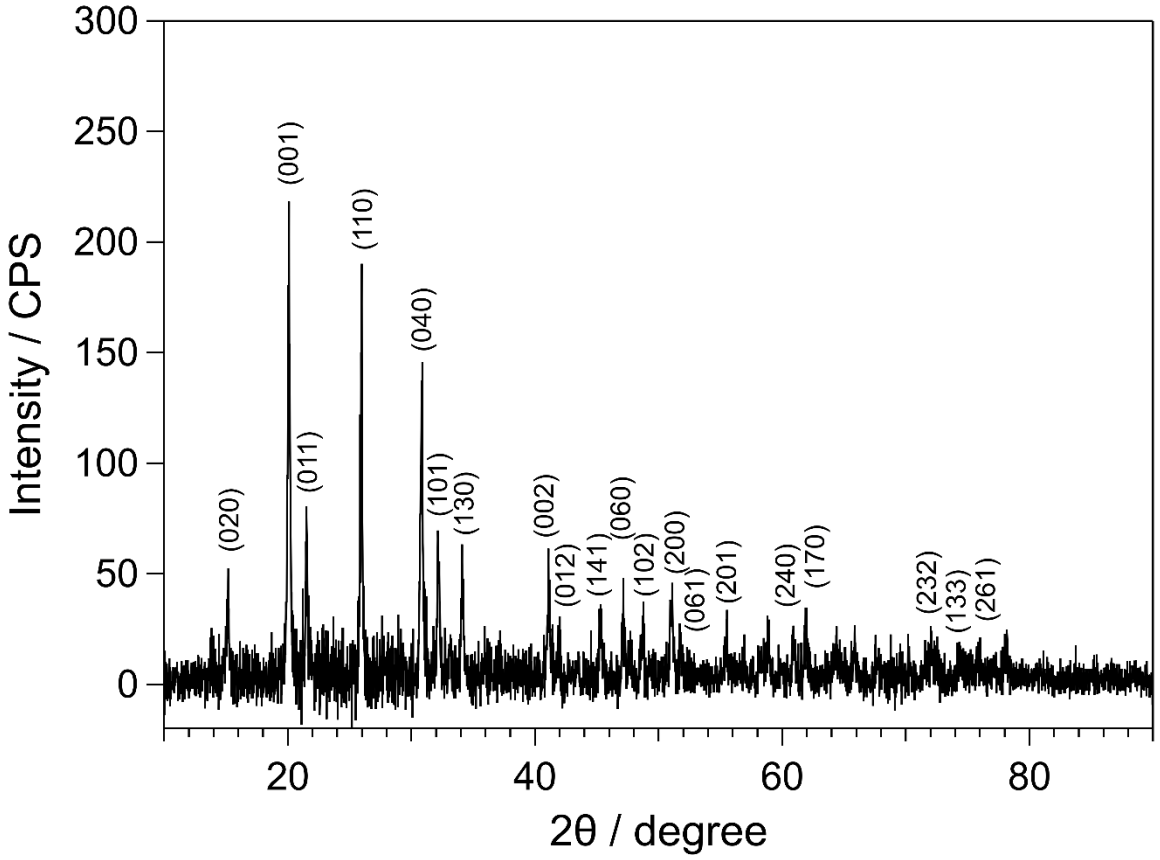

Figure S1-4. XRD pattern of VN nanoparticles post TGA measurement, indicating that VN nanoparticles were oxidized into V_2O_5.

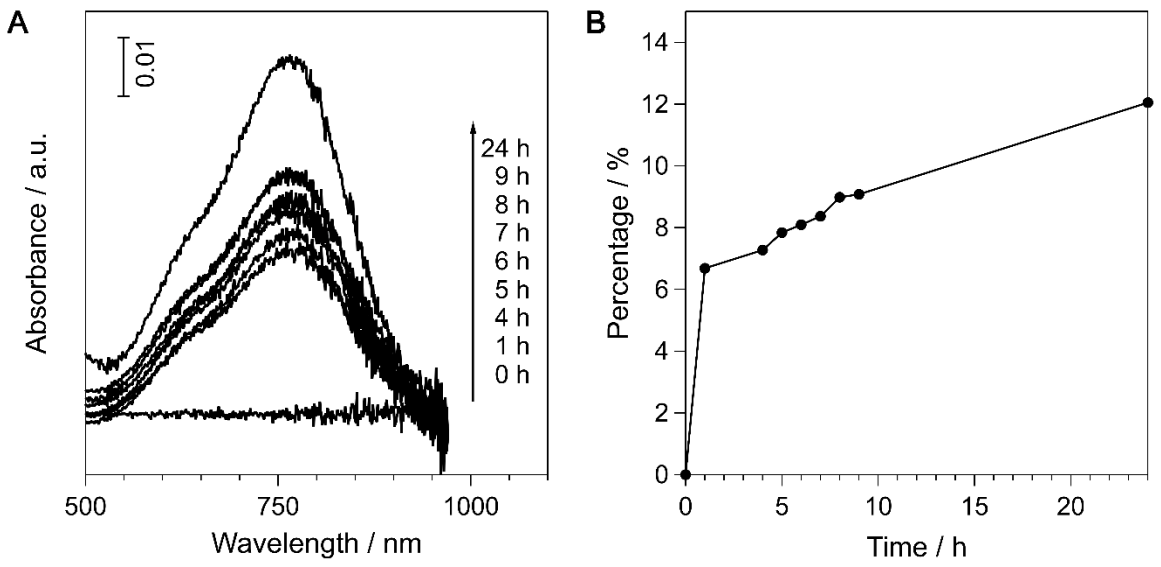

Figure S1-5. Time-dependent UV-vis spectra (A) and degradation rate (B) of VN nanoparticles in 1 M H_2SO_4 at 85 °C, showing the leaching of VO^{2+} from VN nanoparticles.

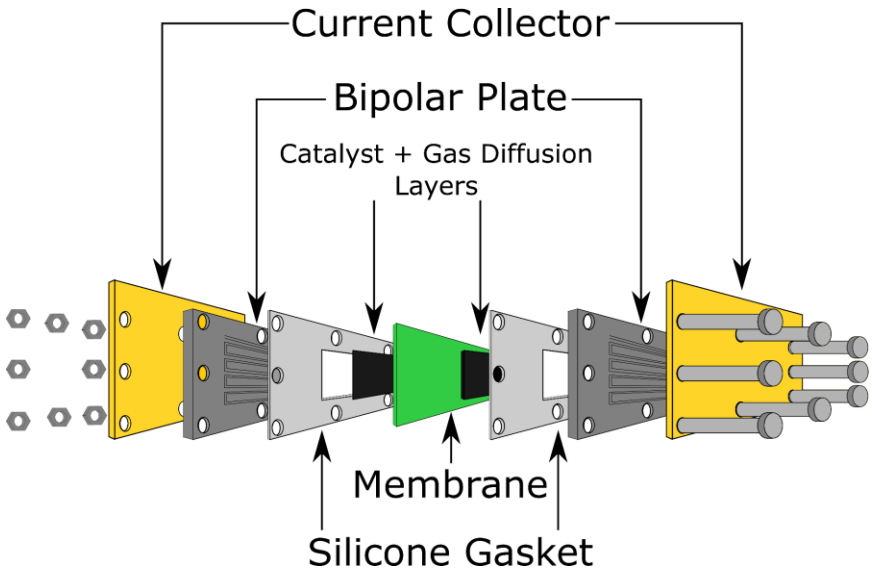

Figure S1-6. Schematic illustration of the MEA configuration used in this work.

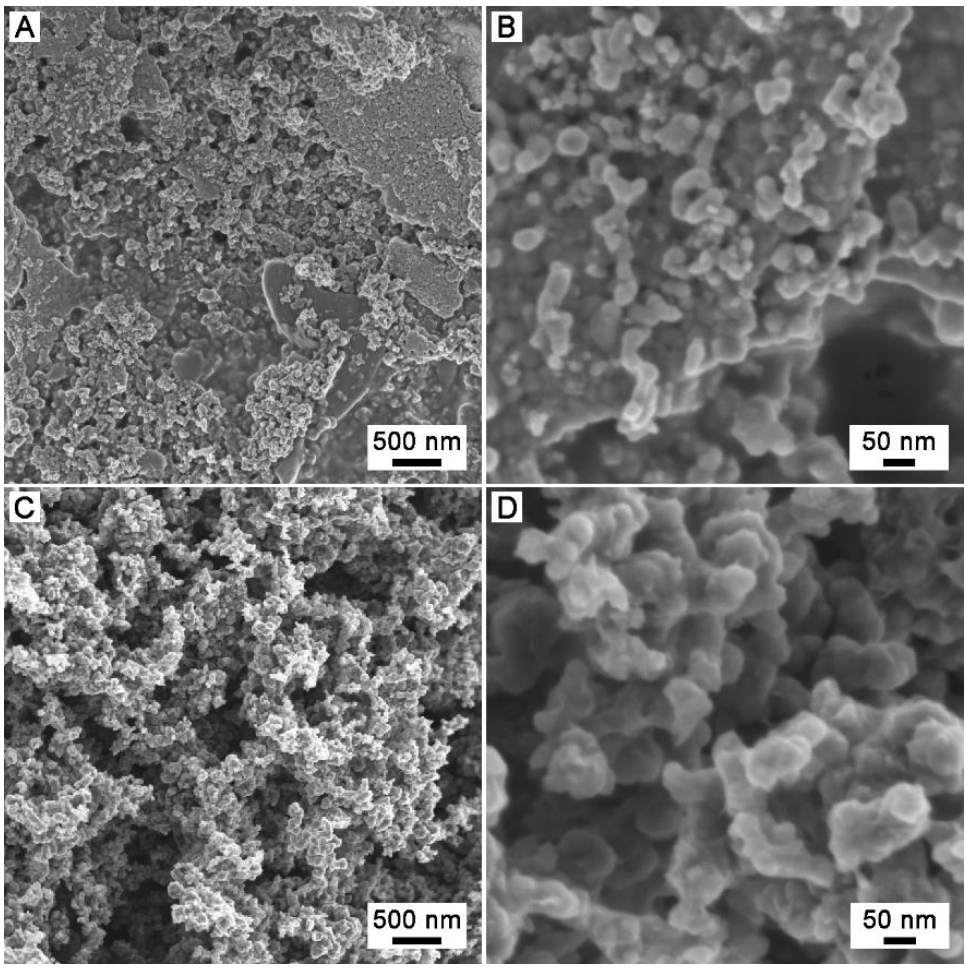

Figure S1-7. SEM images of VN catalysts on carbon paper at different magnifications before (A and B) and after (C and D) nitrogen reduction at −0.2 V for 1 h.

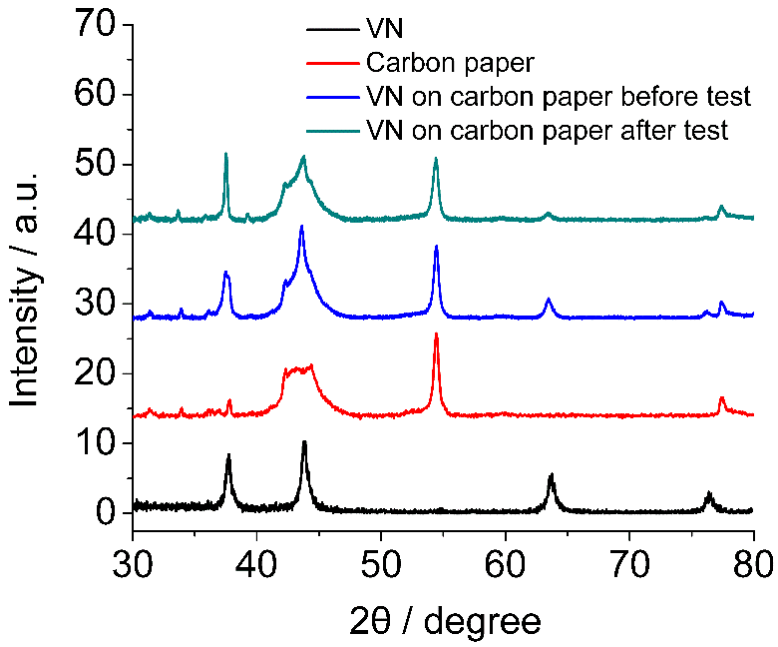

Figure S1-8. XRD patterns of as-synthesized VN nanoparticles, carbon paper, and carbon paper sprayed with VN nanoparticles before and after nitrogen reduction. There are two main diffraction peaks at 43° and 54°, respectively, in the XRD pattern of carbon paper, which is consistent to a previous report.[3]

2. Quantification of Ammonia

The amount of ammonia in the effluent of cathode and anode, as well as in the soaking solution of the spent MEA, was determined using Nessler methods based on the following reaction:

$$NH_4^+ + 2[HgI_4]^{2-} + 4OH^- \rightarrow HgO \cdot Hg(NH_2)I \downarrow + 7I^- + 3H_2O$$

Since the ammonia is collected in acid solutions (cathode/anode effluent and membrane soaking solution), KOH solution (3 M) was added to adjust the pH of the solution to ~12.5. Due to the different concentrations of H_2SO_4 solution used for cathode/anode exhaust (1 mM H_2SO_4) and membrane soaking solution (3 M H_2SO_4), two calibration curves were made by using $(NH_4)_2SO_4$ solutions with known concentrations using a photometer (HI 96715, HANNA) (Figure S2-1A).[4]

Quantification of produced amounts of ammonia in ENRR is based on the mass balance of N in all N-containing species in the system, *i.e.*, VN nanoparticles, ammonia in the cathode and anode effluents, and ammonia trapped in the spent MEA. Due to the possible degradation of VN nanoparticles in the acidic operating environment of PEMELs, the amount of ammonia quantified in the cathode and anode effluents and the MEA soaking solution could originate not only from ENRR, but also from the leaching of N on VN nanoparticles. CHNS Elementar analysis was employed to determine the amount of N in the fresh and spent MEA to determine the change of N content in the MEA before and after ENRR tests.[5,6] The combination of the Nessler method and the Elementar analysis allows us to establish a complete N balance, and the procedure to quantify the amount of ammonia produced *via* ENRR in this work is illustrated in Figure S2-2. Before ENRR tests, VN catalysts on freshly prepared MEA is the only source of nitrogen ($N_{(VN,pre)}$). After ENRR, there are three sources of nitrogen: 1) ammonia in both cathode/anode effluents ($N_{(\mathrm{NH_3,Effluent})}$), 2) ammonia in membrane soaking solution ($N_{(\mathrm{NH_3,MEA})}$), and 3) VN catalysts on the spent MEA ($N_{(\mathrm{VN,post})}$). The amount of ammonia in both cathode/anode effluents and membrane soaking solution were determined using the Nessler method. The N content in both fresh and spent MEAs were determined by the CHNS Elementar analysis. Therefore, the amount of ammonia produced by ENRR is calculated using the following equation based on the mass balance of ENRR:

$$N_{(\mathrm{NH_3,ENRR})} = N_{(\mathrm{NH_3,MEA})} + N_{(\mathrm{NH_3,Effluent})} + N_{(\mathrm{VN,post})} - N_{(VN,pre)}$$

The accuracy of the ammonia quantification method used to calculate ENRR rates and FEs were verified by control experiments. Ammonia was detected in the MEA soaking solution when Ar was fed on the cathode side at different potentials for 1 h, however, no detectable level ammonia was observed in the effluent from either anode or cathode. The amount of ammonia detected in the MEA soaking solution with Ar was independent of the cathodic potential (86.0 ± 12.2 μg, Figure S2-3), which is consistent with NMR results (Figure 2D in the main text). This also agrees with the XPS and XAS results, which suggest that ENRR will convert oxynitride species to VN rather than dissolving VN. When nitrogen gas was introduced at OCP under otherwise identical conditions, no ammonia was detected in cathode or anode effluent. 102.0 ± 11.3 μg of ammonia was detected in the MEA soaking solution, which is close to the amount of ammonia when Ar is fed to the cathode. The nitrogen content in the spent MEA was determined with the CHNS Elementar analysis to be 108.9 ± 30.8 μg ammonia (equivalent of N) less than that of the fresh MEA, which was within the experimental errors of N leached into the soaking solution (102.0 ± 11.3 μg of ammonia equivalent, Figure S2-1B). This control experiment demonstrates that the combination of the Nessler method and the CHNS Elementar analysis is able to establish a quantitatively N balance in the ENRR system, and in turn reliably determine the amount of ammonia produced in ENRR. Table S2-1 shows time-dependent distribution of ammonia during nitrogen reduction. During the first 8 hours nitrogen reduction, most of the produced ammonia was trapped in Nafion membrane and MEA, due to the strong interactions between ammonia and Nafion membrane as well as porous carbon. The amount of ammonia in membrane varies within a narrow range, indicating that the membrane was saturated with ammonia. Therefore, most of produced ammonia was detected in cathode and anode exhausts after 8 hours.

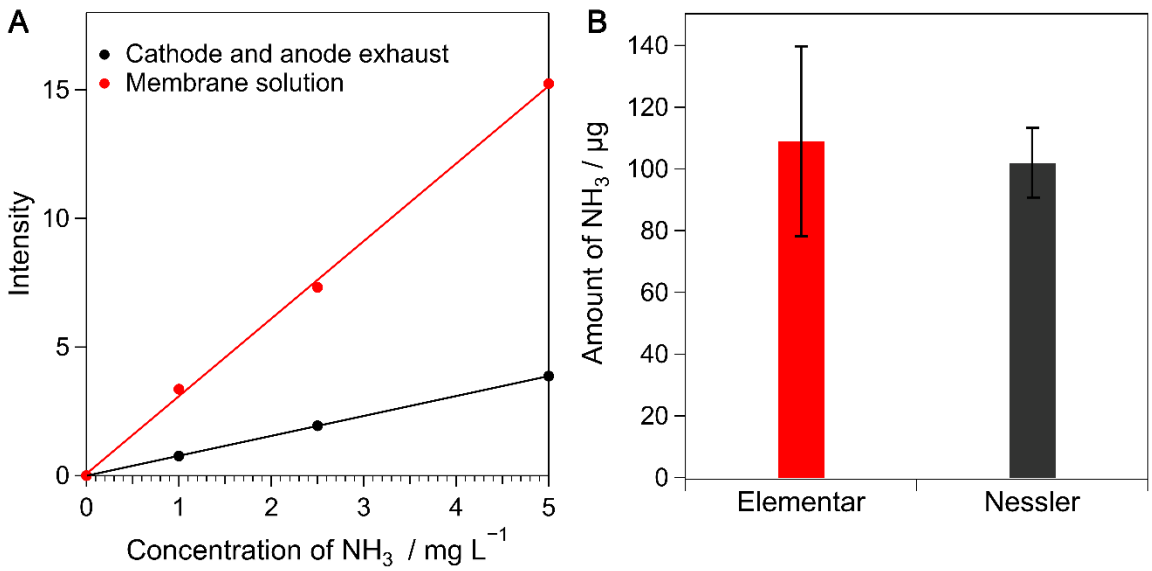

Figure S2-1. (A) Calibration curves for the quantification of ammonia in cathode/anode exhaust and membrane solution. (B) Comparison of ammonia quantifications based on CHNS Elementar analysis and Nessler method.

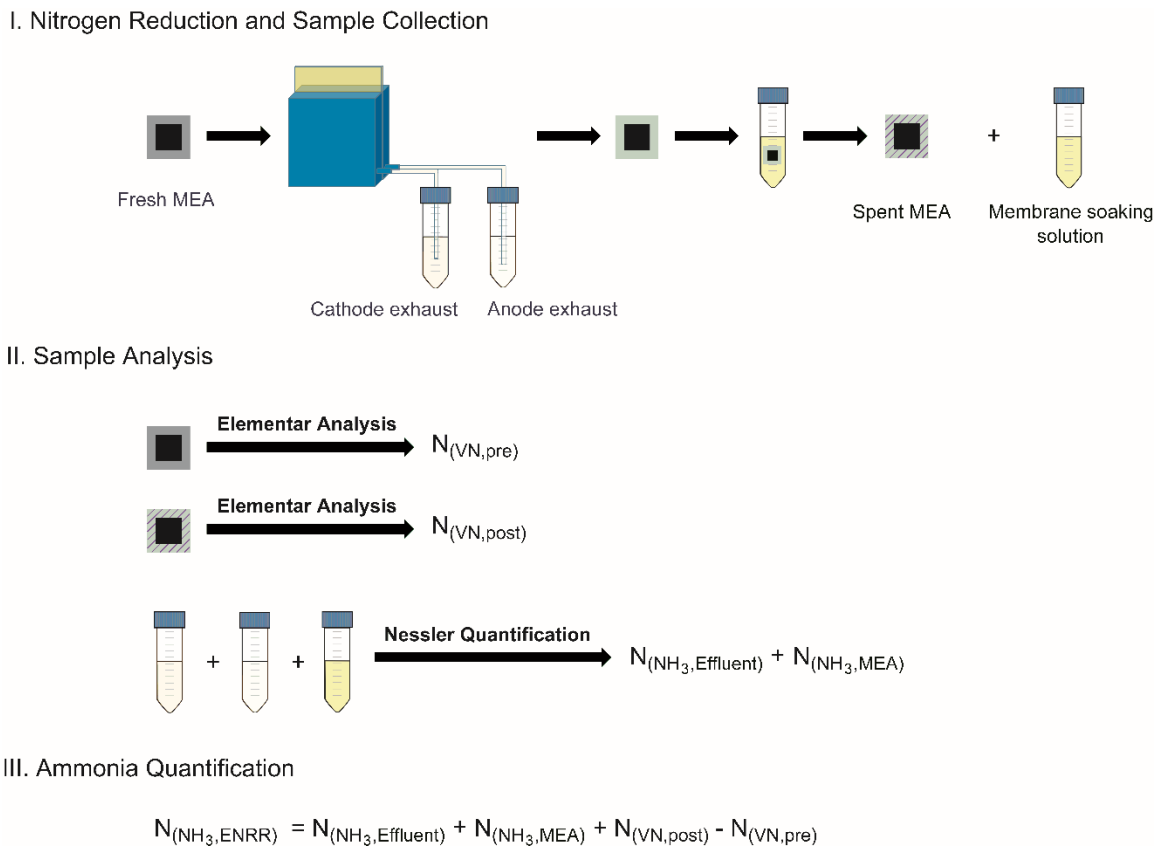

Figure S2-2. Schematic illustration of the procedure to quantify the amount of produced ammonia via nitrogen reduction in this work.

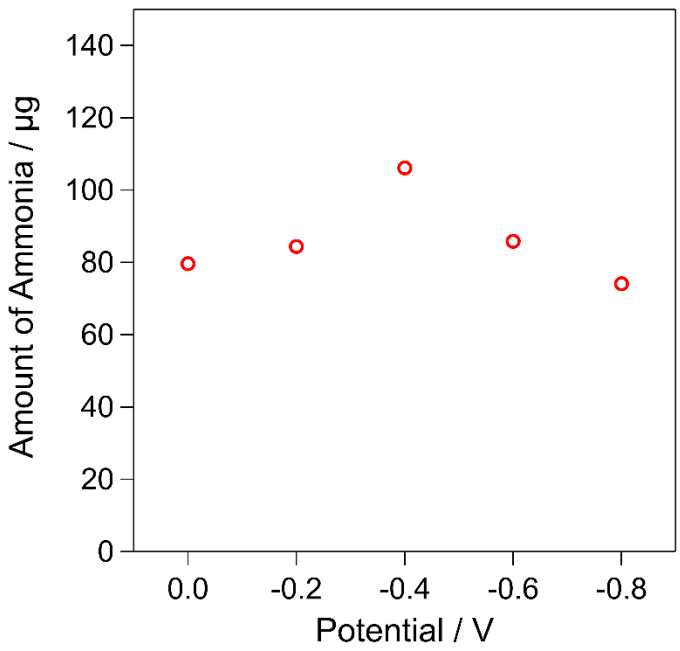

Figure S2-3. The rates of ammonia produced through degradation of the catalysts at different potentials when Ar was fed on the cathode side.

Table S2-1. Time-dependent distributions of ammonia during nitrogen reduction.

Time (h)	$N_{(NH3,Effluent)}$ (μg)	$N_{(NH3,MEA)}$ (μg)	$N_{(VN,post)}$-$N_{(VN,pre)}$ (μg)	Total (μg)
1	0.79	163.57	−63.14	101.22
2	2.49	154.59	47.36	204.44
4	27.79	164.04	157.86	349.69
8	73.94	177.69	252.57	504.20
24	491.29	186.49	378.86	1056.64
48	998.56	200.00	663.00	1861.56
120	2916.99	296.59	1089.13	4302.71

3. Nitrogen Reduction in Batch Mode under $^{15}N_2$

Isotopic labeling experiments with either ^{15}N labeled N_2 or nitrides could pinpoint the source of N in the produced ammonia from ENRR. $^{15}N_2$ was employed as feed in ENRR, and conducted the reaction in a batch cell (Figure S3-1), because it is costly to use $^{15}N_2$ in a flow device like MEA-based electrolyzer. A balloon was used to maintain a slight positive pressure of $^{15}N_2$ in the head space to prevent the $^{14}N_2$ in the atmosphere from leaking into the cell. The isotopic labeling experiment was carried out using the setup with $^{15}N_2$ as the feeding gas in 0.05 M H_2SO_4 electrolyte. After electrolysis at −0.1 V vs. RHE for 48 h, 10 mL of the electrolyte was taken out and concentrated to 1 mL. Then, the electrolyte was mixed with 1 mL of 1M phosphate buffer solution (PBS). 0.9 mL of the resulting solution was taken out and mixed with 0.1 mL D_2O containing 100 ppm DMSO was then added as an internal standard for ^1H nuclear magnetic resonance measurement (^1H NMR, Bruker Avance III 600 MHz).[7] Control experiments at OCP under $^{14}N_2$ and −0.1 V under Ar were conducted following a similar procedure.

Figure S3-2 shows the ^1H NMR results of the ENRR products at −0.1 V for 48 h. There are five peaks corresponding to $^{15}NH_4^+$ and $^{14}NH_4^+$, respectively, indicating that ammonia is produced via electrochemical nitrogen reduction and also ENRR on VN catalysts goes through Mars-van Krevelen mechanism. There is no detectable amount of ammonia produced using commercial Pt/C, Pd/C, and Au/C as catalysts for ENRR under the same conditions, indicating the poor performance of these noble metal catalysts for ENRR.

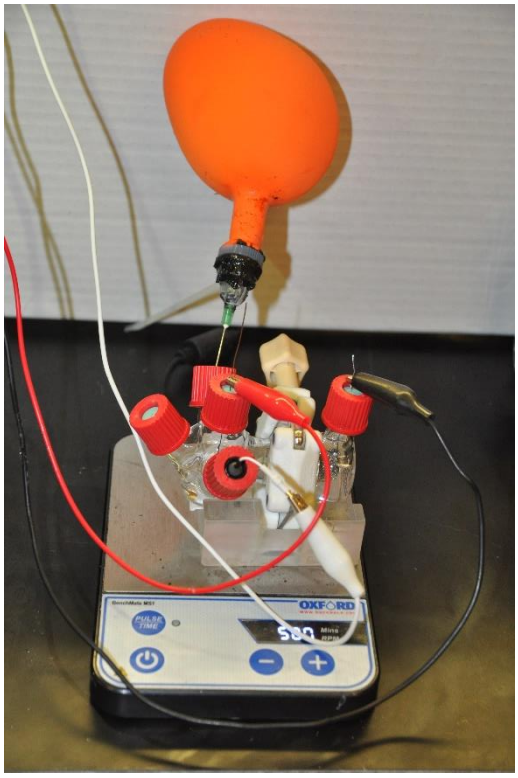

Figure S3-1. The setup for isotopic $^{15}N_2$ experiment with VN catalysts in 0.05 M H_2SO_4. Ag/AgCl and Pt mesh are served as the reference and counter electrodes, respectively.

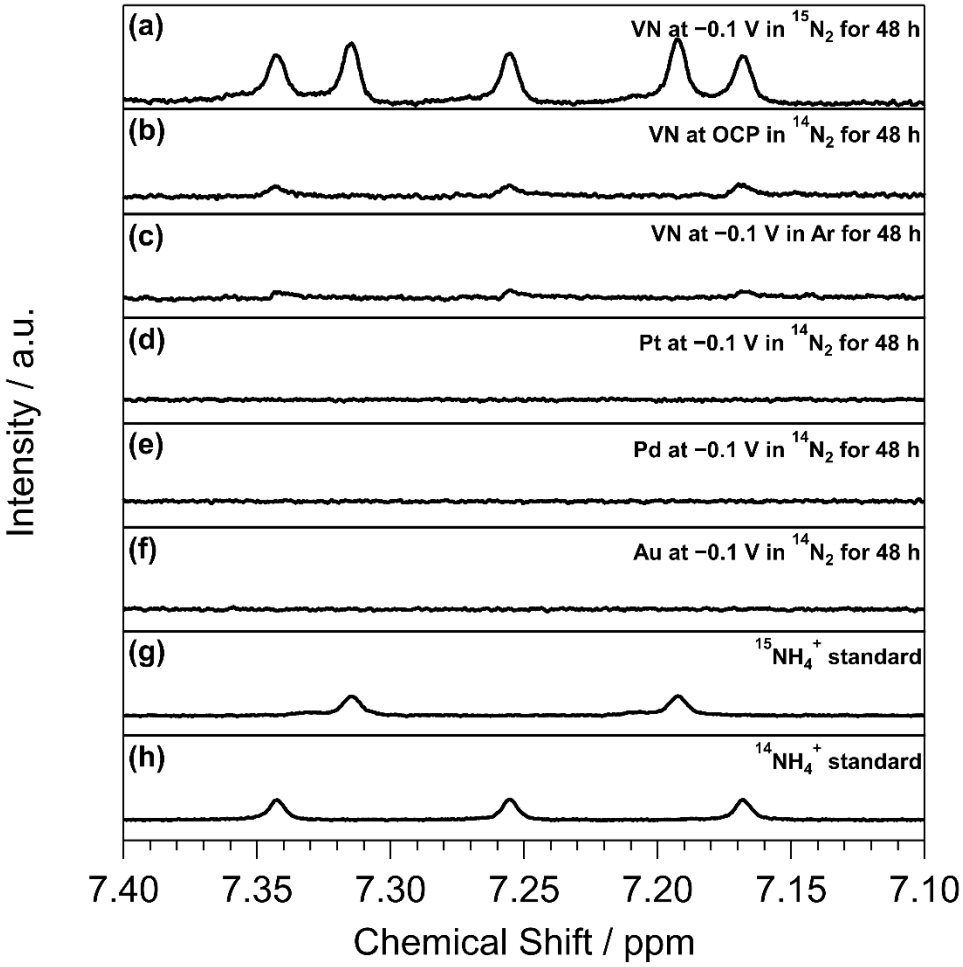

Figure S3-2. ^{1}H nuclear magnetic resonance (NMR) spectra were obtained for the post-electrolysis 0.05 M H_2SO_4 at (a) −0.1 V in $^{15}N_2$, (b) OCP in $^{14}N_2$, and (c) −0.1 V in Ar with VN as catalysts, respectively. ^{1}H NMR spectra were obtained for the post-electrolysis 0.05 M H_2SO_4 at −0.1 V in $^{14}N_2$ with commercial (d) Pt/C, (e) Pd/C, and (f) Au/C as catalysts, respectively. Standard spectra of (g) $^{15}NH_4^+$ and (h) $^{14}NH_4^+$ prepared by dissolving ^{15}N- and ^{14}N-labelled $(NH_4)_2SO_4$ in PBS with a concentration of 100 ppm, respectively. The chemical shifts in the spectra were calibrated using DMSO as an internal standard.

4. Deconvolution of XPS Spectra

All the XPS spectra in this work were deconvoluted using the same set of parameters, with peak assignments consistent with previous reports (Table S4-1 and S4-2). [8–12] The V $2p_{3/2}$ XPS spectra can be deconvoluted into four peaks at 513.6, 515.3, 516.0, and 517.1 eV, which are assigned to V in VN, VN_xO_y, VO_x ($x \leq 2$), and V_2O_5, respectively (Table S4-1). The O 1s band in the range of 530−540 eV is included in all the V 2p spectra in order to obtain a good baseline.[8–10] The N 1s XPS spectra could also be deconvoluted into four bands, with the band at 397.3 eV being assigned to N in VN.[9,11,12] A 1:1 ratio between the bands assigned to V and N in VN (corrected with atomic sensitivity factors) is maintained in the peak fitting for all XPS spectra in this work. The other three N 1s peaks at 396.4, 398.4, and 401.0 eV are assigned to the VN_xO_y, a satellite peak, and ammonia/ammonium species, respectively, based on literature (Table S4-2).[9,11,12]

Table S4-1. The parameters for the deconvolutions of V 2p spectra.

Specie	Band	Position (eV)	Full Width at Half Maximum (eV)	Reference
VN	$2p_{3/2}$	513.63	1.75	8−10
	$2p_{1/2}$	521.10	1.75	
VN_xO_y	$2p_{3/2}$	515.09	1.92	9
	$2p_{1/2}$	522.47	1.92	
VO_x ($x \leq 2$)	$2p_{3/2}$	515.99	1.48	8−10
	$2p_{1/2}$	523.31	1.48	
V_2O_5	$2p_{3/2}$	517.10	1.36	8−10
	$2p_{1/2}$	524.41	1.57	

Table S4-2. The parameters for the deconvolutions of N 1s spectra.

Specie	Band	Position (eV)	Full Width at Half Maximum (eV)	Reference
VN	N 1s	397.3	0.80	9−11
VN_xO_y	N 1s	396.4	1.05	9,10
Satellite peak	N 1s	398.4	2.00	9
ammonia/ammonium	N 1s	401.0	2.33	12

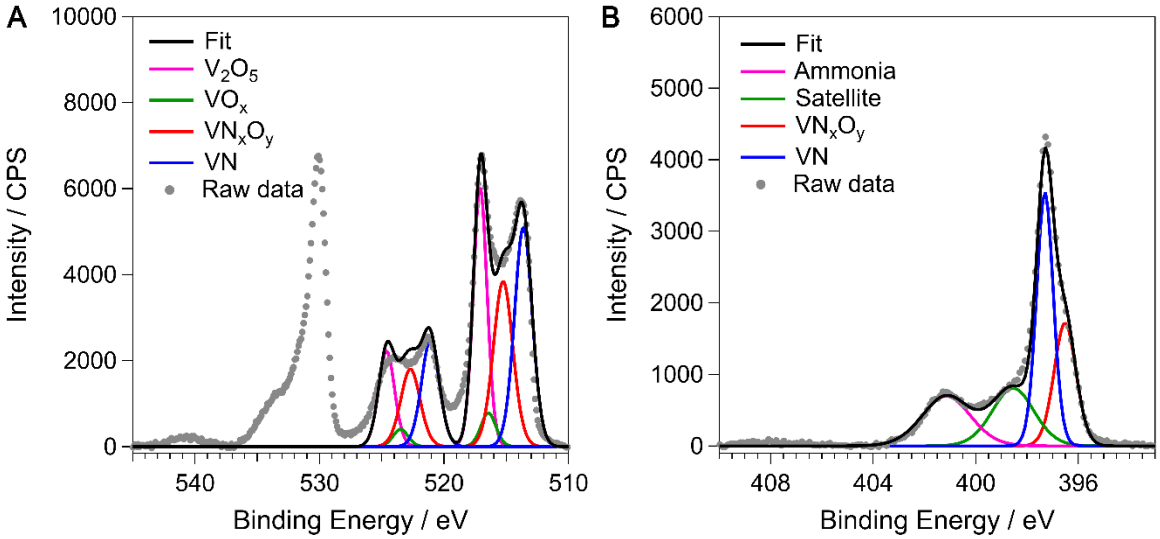

Figure S4-1. XPS deconvolutions of the V 2p region (A) and N 1s region (B) of VN catalysts on carbon paper before nitrogen reduction.

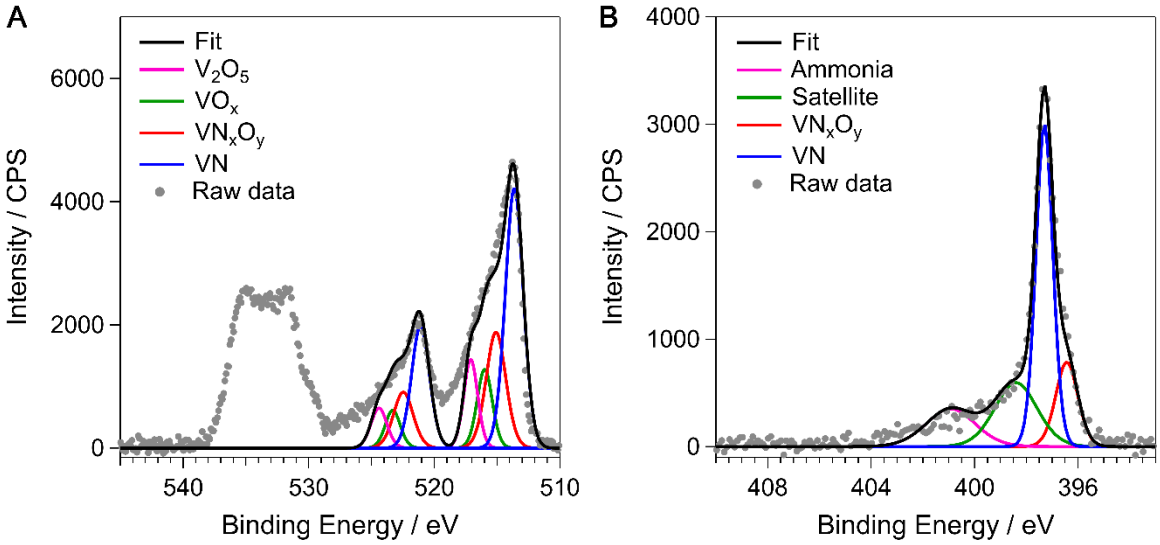

Figure S4-2. XPS deconvolutions of the V 2p region (A) and N 1s region (B) of VN catalysts after nitrogen reduction at −0.2 V for 1 h.

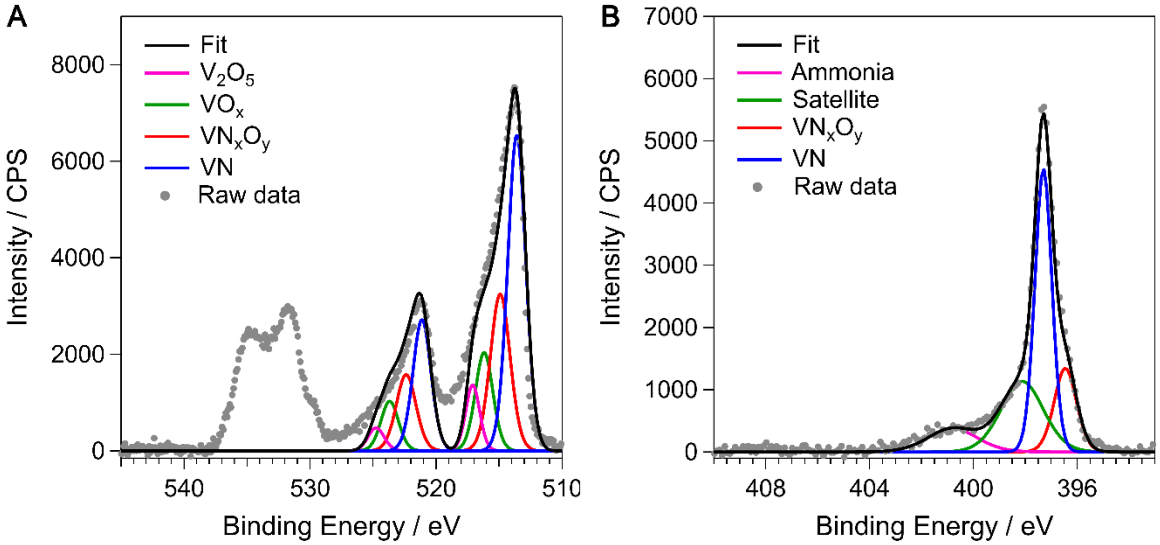

Figure S4-3. XPS deconvolutions of the V 2p region (A) and N 1s region (B) of VN catalysts after nitrogen reduction at −0.4 V for 1 h.

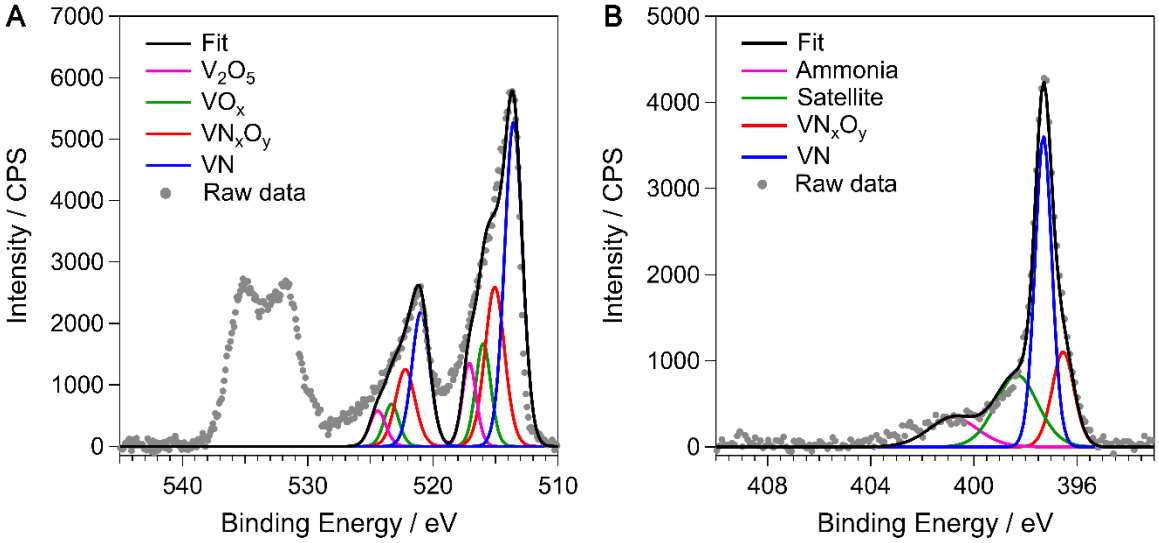

Figure S4-4. XPS deconvolutions of the V 2p region (A) and N 1s region (B) of VN catalysts after nitrogen reduction at −0.6 V for 1 h.

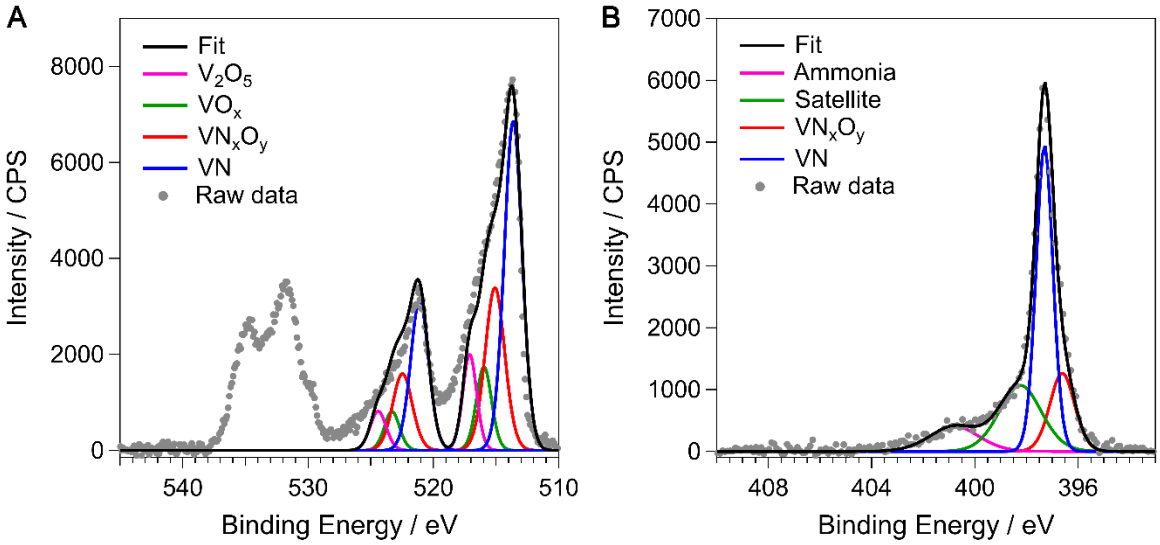

Figure S4-5. XPS deconvolutions of the V 2p region (A) and N 1s region (B) of VN catalysts after nitrogen reduction at −0.8 V for 1 h.

5. *Operando* XAS Characterizations of VN Catalysts

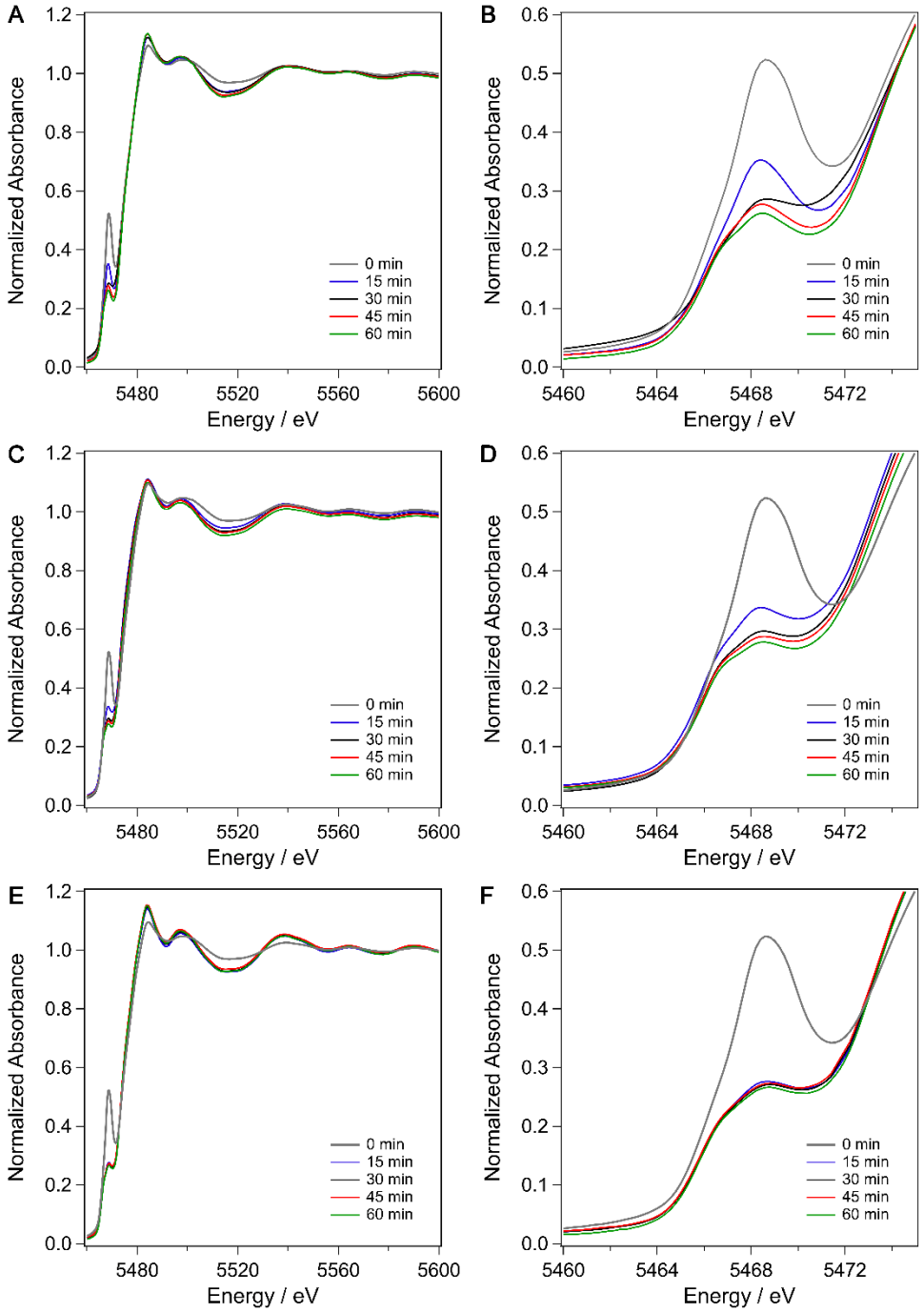

Figure S5-1. *Operando* XAS results of VN catalysts: K-edge XANES spectra of VN catalysts at different potentials (A) −0.4 V, (C) −0.6 V, and (E) −0.8 V. The corresponding pre-edge peaks at different potentials (B) −0.4 V, (D) −0.6 V, and (F) −0.8 V.

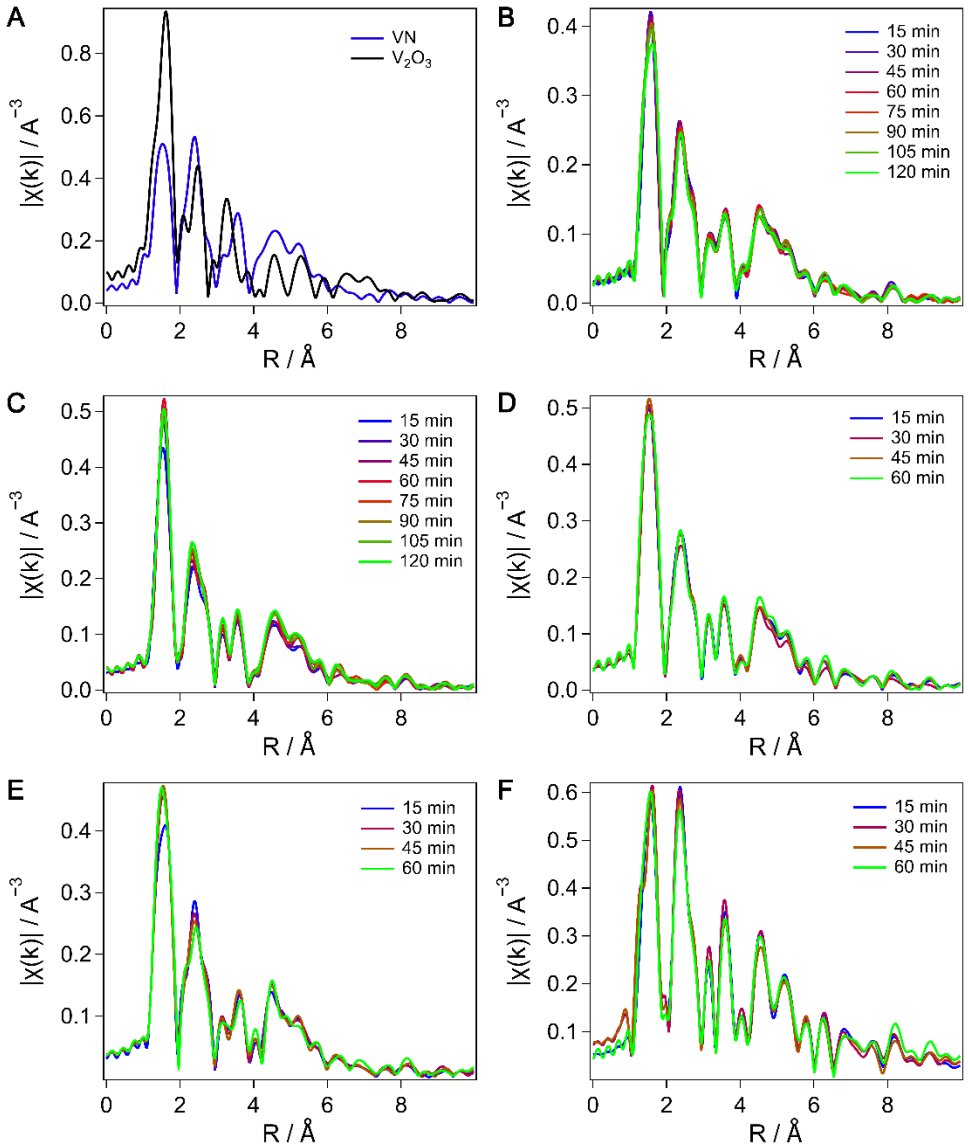

Figure S5-2. (A) XAFS results of standard samples, including VN nanoparticles and V_2O_3. Time-dependent XAFS results of VN catalysts during nitrogen reduction at different potentials: (B) −0.1 V, (C) −0.2 V, (D) −0.4 V, (E) −0.6 V, and (F) −0.8 V.

6. Production Rate and FE of Other ENRR Catalysts

Table S6-1. Production rate and Faradaic efficiency when V_2O_3 was employed as catalysts for nitrogen reduction at −0.2 V for 1 h.

Production Rate (10^{-10} mol s^{-1} cm^{-2})	**Faradaic Efficiency (%)**
0.54 ± 0.10	0.34 ± 0.07

Table S6-2. List of previously reported production rate and FE of ENRR catalysts.

Cathode	Anode	Electrolyte	Production Rate (mol cm^{-2} s^{-1})	FE	j_{NRR} (μA cm^{-2})	Potential (vs NHE)	Reference
Fe electrode	Stainless Steel	6N KOH	0.6×10^{-14}	n.a.	n.a.	−0.85 V	13
Ru/C	Pt	Nafion	3.43×10^{-12}	0.28%	n.a.	−0.9 V	14
Pt/C	Pt	Nafion	1.14×10^{-9}	0.55%	1050	0.2 V vs RHE	15
Fe/CNT	Pt	Nafion/GDL	3.59×10^{-12}	0.03%	1.2	−2.0 V	16
Au NR	Pt	0.1 M KOH/Nafion	2.69×10^{-11}	4.00%	10	−0.97 V	17
Au/TiO2	Pt	HCl/Nafion	5.94×10^{-9}	8.11%	35	−0.2 V vs RHE	18
Au-CeOx/RGO	Pt	HCl/Nafion	1.35×10^{-10}	10.10%	10	−0.2 V vs RHE	19
Polyimide/C	Pt	Li^+/H^+	7.68×10^{-12}	2.91%	<10	−0.4 V vs RHE	20
Mo nanofilm	Pt	0.01 M H_2SO_4	3.09×10^{-11}	0.72%	5.5	−0.39 V vs RHE	21
Ir/C	Pt/C	Nafion	2.09×10^{-12}	0.02%	0.60	−0.2 V vs RHE	22
VN NPs	**Pt/C**	**Nafion**	**3.31×10^{-10}**	**5.95%**	**95.8**	**−0.1 V vs RHE**	**This work**

Practical NRR current: $j_{NRR} = j_{operational} \times \mathrm{FE}$

7. Computational Methods

DFT calculations were performed to compare the effect of oxygen modification on the binding strength of H and N on VN(111) and $VN_{0.75}O_{0.25}$(111) surfaces. As shown in Table S7-1, the H and N binding energies are not significantly affected on the N vacancy sites of the two surfaces. However, the O vacancy site on $VN_{0.75}O_{0.25}$(111) binds to N much more strongly, about 2.51 eV and 2.36 eV stronger than that on N vacancy of VN(111) and VNO(111), respectively, while the H binding energy increases only slightly, by 0.32 eV and 0.28 eV, respectively. The different extent of increase in H and N binding energies suggests that the formation of oxynitride offers the possibility of breaking the linear scaling relationship between the two adsorbates, which might be responsible for the enhanced ENRR activity.

Spin polarized density functional theory (DFT)[23,24] calculations were performed at the GGA level within the PAW-PW91 formalism[25,26] using the Vienna Ab-Initio Simulation Package (VASP) code.[27,28] The bulk vanadium nitride (VN) was modeled using a cubic NaCl structure. The DFT calculated lattice parameter of bulk VN was 4.12 Å which is in close agreement with the experimental value of 4.14 Å and previously calculated lattice parameter with similar methods.[29] The bulk vanadium oxynitride (VNO) with 25% O concentration (*i.e.*, $VN_{0.75}O_{0.25}$) was modeled by replacing one N atom in the unit cell of bulk VN with an O atom. The DFT calculated lattice parameter of bulk VNO in the present study is 4.14 Å which agrees well with previously calculated lattice parameter of similar structure with similar methods.[29]

The N-terminated-VN(111) and NO-terminated-VNO(111) surfaces were modeled using six layer 4 × 4 surface slabs. The Brillion zone integration was performed using a 3 × 3 × 1 Monkhorst-Pack grid[30] and a plane wave cut-off energy of 400 eV was used for the total energy calculations. A vacuum layer of ~15 Å thick was added in the slab cell along the direction perpendicular to the surface in order to minimize the artificial interactions between the surface and its periodic images. During geometry optimization, atoms in the top three layers were allowed to relax while atoms in the bottom three layers were fixed

until the Hellman-Feynman force on each ion was smaller than 0.01 eV/Å. The binding energy (BE) of an adsorbate was calculated as:

$$BE(adsorbate) = E(slab + adsorbate) - E(slab) - E(adsorbate)$$

where E(slab + adsorbate), E(slab) and E(adsorbate) are the total energy of slab with adsorbate, the energy of clean slab and the energy of adsorbate in the gas phase, respectively.

Table S7-1. DFT calculated H and N binding energies (in eV) on VN(111) and $VN_{0.75}O_{0.25}$(111) surfaces.

	VN(111)	VNO(111)	
Adsorbates	N-vacancy	N-vacancy	O-vacancy
H	-2.63	-2.67	-2.95
N	-4.90	-5.05	-7.41

8. Turnover Number of the Catalysts

The total amount of produced ammonia was determined to be 253.1 μmol at −0.1 V within 120 h. Based on XPS analysis, x and y in VN_xO_y phase were determined to be 0.7 and 0.45, respectively.

Based on the Elementar analysis results (Table S1-1), the total amount of VN and $VN_{0.7}O_{0.45}$ in the catalysts was:

$$1 - 16.85\ wt\% = 83.15\ wt\%$$

Also, the total N content in the catalysts was 15.51 wt% (Table S1-1). Since there was 2.5 mg of the catalysts on carbon paper, the amount of active phase ($VN_{0.7}O_{0.45}$) for nitrogen reduction was:

$$2.5 \times 10^{-3} g \times \frac{\frac{0.8315}{(51+14)\ g/mol} - \frac{0.1551}{14\ g/mol}}{\frac{(51 + 0.7 \times 14 + 0.45 \times 16)\ g/mol}{(51+14)\ g/mol} - \frac{(14 * 0.7)\ g/mol}{14\ g/mol}} = 12.4\ \mu mol$$

Therefore, the turnover number (TON) of the catalysts within 120 h was determined to be:

$$\frac{253.1\ \mu mol}{12.4 \times 0.7\ \mu mol} = 29.2$$

Based on XAS results, 57.8% of the active phase (*i.e.*, 7.2 μmol) was converted to VN during nitrogen reduction, which is corresponding to 5.0 μmol of active nitrogen atoms. Thus, the total amount of active nitrogen atoms in the catalysts after 4 h was:

$$12.4 \times (1 - 57.8\%) \times 0.7\ \mu mol = 3.7\ \mu mol$$

Since the total amount of ammonia produced at −0.1 V from 5 to 120 h was determined to be 232.5 μmol. the turnover number (TON) of the catalysts at steady state (5−120 h) was determined to be:

$$\frac{232.5\ \mu mol}{3.7\ \mu mol} = 62.8$$

Reference

1. Zheng, J.; Sheng, W.; Zhuang, Z.; Xu, B.; Yan, Y. *Sci. Adv.* **2016**, *2*, e1501602.
2. Giordano, C.; Erpen, C.; Yao, W.; Milke. B.; Antonietti, M. *Chem. Mater.* **2009**, *21*, 5136−5144.
3. Si, Q.; Matsui, M.; Horiba, T.; Yamamoto, O.; Takeda, Y.; Seki, N.; Imanishi, N. *J. Power Sources* **2013**, *241*, 744−750.
4. Tang, X.; Wu, Q. Y.; Du, Y.; Yang, Y.; Hu, H. Y. *Water Res.* **2014**, *48*, 490−497.
5. Gondek, K.; Mierzwa-Hersztek, M. *Soil Use Manage.* **2016**, *32*, 357−367.
6. Gondek, K.; Mierzwa-Hersztek, M.; Kopeć, M. *J. Environ. Manage.* **2018**, *210*, 87−95.
7. Wang, J.; Yu, L.; Hu, L.; Chen, G.; Xin, H.; Feng, X. *Nat. Commun.* **2018**, *9*, 1795.
8. Silversmit, G.; Depla, D.; Poelman, H.; Marin, G. B.; De Gryse, R. *J. Electron. Spectrosc. Relat. Phenom.* **2004**, *135*, 167−175.
9. Glaser, A.; Surnev, S.; Netzer, F. P.; Fateh, N.; Fontalvo, G. A.; Mitterer, C. *Surf. Sci.* **2007**, *601*, 1153−1159.
10. Zhao, D.; Cui, Z.; Wang, S.; Qin, J.; Cao, M. *J. Mater. Chem. A* **2016**, *4*, 7914−7923.
11. Saha, N. C.; Tompkins, H. G. M. *J. Appl. Phys.* **1992**, *72*, 3072−3079.
12. Wagner C. D.; Naumkin, A. V.; Kraut-Vass, A.; Allison, J. W.; Powell, C. J.; Rumble, J. R. Jr.; NIST Standard Reference Database 20, Version 3.4 (web version) **2003**.
13. Sclafani, A.; Augugliaro, V.; Schiavello, M. *J. Electrochem. Soc.* **1983**, *130*, 734−736.
14. Kordali, V.; Kyriacou, G.; Lambrou, C. *Chem. Commun*. **2000,** *0*, 1673−1674.
15. Lan, R.; Irvine, J. T. S.; Tao, S. *Sci. Rep.* **2013,** *3,* 1145.
16. Chen, S.; Perathoner, S.; Ampelli, C.; Mebrahtu, C.; Su, D.; Centi, G. *Angew. Chem. Int. Ed*. **2017,** *56,* 2699−2703.
17. Bao, D.; Zhang, Q.; Meng, F.-L.; Zhong, H.-X.; Shi, M.-M.; Zhang, Y.; Yan, J.-M. ; Jiang, Q.; Zhang, X.-B. *Adv. Mater.* **2017,** *29,* 1604799.
18. Shi, M.-M.; Bao, D.; Wulan, B.-R.; Li, Y.-H.; Zhang, Y.-F.; Yan, J.-M.; Jiang, Q. *Adv. Mater.* **2017,** *29,* 1606550.

19. Li, S.-J.; Bao, D.; Shi, M.-M.; Wulan, B.-R.; Yan, J.-M.; Jiang, Q. *Adv. Mater.,* **2017,** *29,* 1700001.
20. Chen, G.-F.; Cao, X.; Wu, S.; Zeng, X.; Ding, L.-X.; Zhu, M.; Wang, H. *J. Am. Chem. Soc*. **2017,** *139,* 9771−9774.
21. Yang, D.; Chen, T.; Wang, Z. *J. Mater. Chem. A* **2017,** *5,* 18967−18971.
22. Nash, J.; Yang, X.; Anibal, J.; Wang, J.; Yan, Y.; Xu, B. *J. Electrochem. Soc.* **2017**, *164*, F1712−F1716.
23. Hohenberg, P.; Kohn, W. *Phys. Rev.* **1964**, *136*, B864−B871.
24. Kohn, W.; Sham, L. J. *Phys. Rev.* **1965**, *140*, A1133−A1138.
25. Blöchl, P. E. *Phys. Rev. B* **1994**, *50*, 17953−17979.
26. Perdew, J. P.; Wang, Y. *Phys. Rev. B* **1992**, *45*, 13244−13249.
27. Kresse, G.; Furthmüller, J. *Comp. Mater. Sci*. **1996**, *6*, 15−50.
28. Kresse, G.; Hafner, J. *Phys. Rev. B* **1993**, *48*, 13115−13118.
29. de Souza, E. F.; Chagas, C. A.; Ramalho, T. C.; da Silva, V. T.; Aguiar, D. L. M.; San Gil, R.; de Alencastro. R. B. *J. Phys. Chem. C* **2013**, *117*, 25659−25668
30. Monkhorst, H. J.; Pack, J. D. *Phys. Rev. B* **1976**, *13*, 5188−5192.